東北大学機関リポジトリ
TOUR
Tohoku University Repository
東北大学

Multidimensional analysis method for NOAA AVHRR images

著者	工藤　純一
journal or publication title	IEEE Transactions on Geoscience and Remote Sensing
volume	32
number	4
page range	949-954
year	1994
URL	http://hdl.handle.net/10097/47520

doi: 10.1109/36.298025

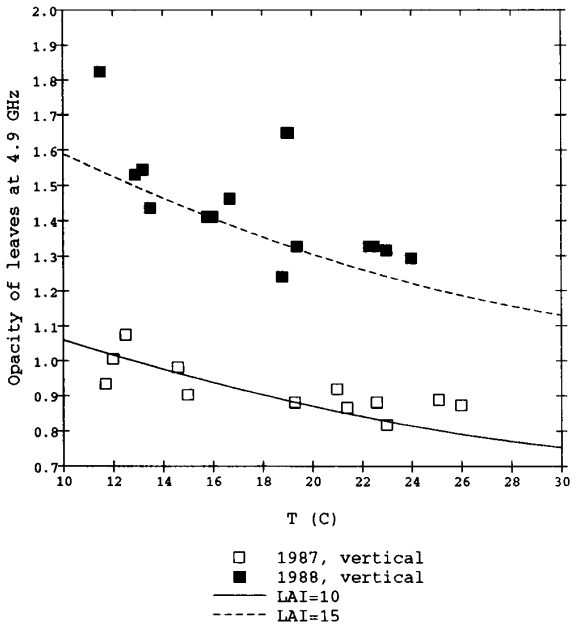

Fig. 3. Temperature dependence of the opacity due to the leaves of a beech at 4.9 GHz. The open symbols are measured data from 1987, the full symbols those of 1988, and the two curves are computed values based on (7) and (8) with $A_p = 1$ and LAI = 10 and 15, respectively; $m_d = 0.26$ and $d = 0.1$ mm.

in this case $A_p = 1$ [10]. Since $k = 1.03$/cm the only unknown quantity is LAI. We only know that LAI was larger in 1988 by a factor of about 1.5 [3]. If we assume LAI = 10 for the 1987 data and LAI = 15 for the 1988 data we obtain the solid and dashed curves, respectively. These LAI values are quite high. However, since the sun leaves near the top are thicker than the modeled shade leaves, the result does not appear unreasonable. Also, the temperature variation modeled by (7) and (8) agree with the observed behavior.

IV. Concluding Remarks

The derivation of a formula for the permittivity of fresh leaves leads to (7), which only depends on two explicit variables, namely m_d and ϵ_{SW}. This formula is simpler than an earlier expression derived by Ulaby and El Rayes [8], where density was an additional parameter, and where an effect by bound water was hypothesized. According to the observations of Sume *et al.* [7] and of Mätzler and Sume [4], the density of fresh leaves of all the observed plants is between 0.9 and 1.0 g/cm^3. Therefore density does not seem to be a significant variable for leaves. On the other hand, the hypothesized behavior of the bound-water relaxation [8] does not seem to fit the observations of Mätzler and Sume [4]. Therefore, in the present case of leaves with a high water content, we adopted the new and simpler approximation. It is clear that bound-water effects would have to be considered for dryer leaf material.

The fact that (7) not only fits the frequency behavior over the entire 1–100 GHz range, but also follows the correct temperature variation at 4.9 GHz, puts confidence in the validity of this new formula.

In the future the test of the temperature dependence should be extended to higher frequencies with more sophisticated propagation models. Further tests should include other vegetation elements, such as needles and stalks and the influence of variable salinity.

Acknowledgment

The author wishes to thank F. Ulaby and U. Wegmüller for helpful discussions on the subject of this paper, and F. Ulaby for sending me the detailed report [2].

References

[1] M. A. El Rayes and F. T. Ulaby, "Microwave dielectric spectrum of vegetation—Part I: Experimental observations," *IEEE Trans. Geosci. Remote Sens.*, vol. GE-25, pp. 541–549, 1987.

[2] ——, "Microwave dielectric behaviour of vegetation material," NASA GSFC Rep., Contract NAG 5-480, Jan. 1987.

[3] C. Mätzler, "Microwave transmissivity in forest canopy: Experiments made with a beech," *Remote Sens. Environ.*, in press, 1994.

[4] C. Mätzler and A. Sume, "Microwave radiometry of leaves," in *Microwave Radiometry and Remote Sensing Applications*, P. Pampaloni, Ed. Utrecht, The Netherlands: VSP, 1989, pp. 133–148.

[5] C. Mätzler and U. Wegmüller, "Progress in multi-frequency radiometry of natural objects," in *Proc. ESA-NASA Workshop Passive Microwave Remote Sens. Res. Related to Land-Atmosphere Interact.*, St. Lary, France, Jan. 10–15, 1993.

[6] D. Polder and J. H. van Santen, "The effective permeability of mixtures of solids," *Physica*, vol. 12, no. 5, pp. 257–271, 1946.

[7] A. Sume, C. Mätzler, R. Hüppi, and E. Schanda, "Microwave radiometer and scatterometer measurements of vegetation," FOA Rep. C30494-3.2, ISSN 0347-3708, Swedish Def. Res. Establish., Linköping, Sweden, 1988.

[8] F. T. Ulaby and M. A. E. Rayes, "Microwave dielectric spectrum of vegetation—Part II: Dual-dispersion model," *IEEE Trans. Geosci. Remote Sens.*, vol. GE-25, pp. 550–557, 1987.

[9] F. T. Ulaby, R. K. Moore, and A. K. Fung, *Microwave Remote Sensing, Active and Passive*, vol. 3. Dedham, MA: Artech House, 1986.

[10] U. Wegmüller, C. Mätzler, and E. Njoku, "Canopy opacity models," in *Proc. ESA-NASA Workshop Passive Microwave Remote Sens. Res. Related Land-Atmosphere Interact.*, St. Lary, France, Jan. 10–15, 1993.

Multidimensional Analysis Method for NOAA AVHRR Images

Jun-ichi Kudoh, Goutam Chakravorty, Yoshiaki Nemoto, Norio Shiratori, Hiroshi Kawamura, Seijiro Obata, and Shoichi Noguchi

***Abstract*—As a fundamental study of multiple image processing, we have developed a new technique for the analysis of multispectral remote sensing data. Though the basis of our algorithm is similar to a**

Manuscript received June 2, 1992; revised March 17, 1993 and March 29, 1994

J.-I. Kudoh and Y. Nemoto are with the Computer Center, Tohoku University, Sendai, Japan.

G. Chakravorty and N. Shiratori are with the Research Center for Electrical Communication, Tohoku University, Sendai, Japan.

H. Kawamura is with the Faculty of Science, Tohoku University, Sendai, Japan.

S. Obata is with the Sendai National College of Technology, Sendai, Japan.

S. Noguchi is with the Faculty of Engineering, Nihon University, Kooriyam, Japan.

IEEE Log Number 9402668

0196-2892/94$04.00 © 1994 IEEE

Authorized licensed use limited to: TOHOKU UNIVERSITY. Downloaded on March 08,2010 at 01:43:09 EST from IEEE Xplore. Restrictions apply.

histogram analysis, we have proposed a novel way of the representation of multidimensional image data, which facilitates a nonexpert to locate and assign different classes present in the data set. Our experimentation was done with NOAA satellite image data. Here, the brightness of the received data from channels of different frequency bands are the different dimensions of the multispectral image. By using our method, we could successfully classify NOAA satellite data received from the northern part of Japan, and located the plane areas as an exercise. We quantitatively compared our result with official data and our result was found to be only 1 percent in deviation with the official data.

I. Introduction

For image analysis, to classify multidimensional data in a spatial distribution, it is necessary to classify data according to some resemblance or closeness. The previous methods of clustering, namely the Karhunen–Loeve transform or the conventional pattern recognition methods, calculate the distance of the different sample vectors in the multidimensional spatial distribution. When the dimension is high and the amount of data is large (as with satellite data), computation almost beyond the scope of ordinary computers is required [1]. Histogram analysis is a possible approach.

In the previous work of three-dimensional histogram analysis by C. E. Livingstone *et al.* [2], elliptical clusters were assumed. In other related works [3]–[5] some *a priori* knowledge of clusters were presumed. In our previous work [6], [7] no such restriction of cluster shapes, or *a priori* knowledge of clusters was required.

In our previous work, we used the NOAA (National Oceanic and Atmospheric Administration) AVHRR (advanced very high resolution radiometer) image data [8], [9], and reported how to identify the location and area of fog from three-dimensional histogram images. There x, y, and z axes of the image histogram directly corresponded to the three-image channel data, respectively. We proposed a simple, user-friendly method to identify clusters from a three-dimensional histogram, which can be used by nonexperts.

Our previous work had the following drawbacks. It could only cope with three-dimensional data. This is a strong restriction, as with present-day satellites, we can receive many channels of data simultaneously. Also, the separation boundaries of the different classes are not very clear. A human factor was involved in demarcating the difference clusters. In this communication, we propose a new method for the segregation of multichannel data into distinctly separate groups. The algorithm poses no restriction on the number of channels that could be analyzed. In this method, the different groups of data form distinct clusters on the visual screen. So, the human factor involved in correctly separating the different clusters is very low, and is therefore suitable for nonexperts.

In this work, instead of plotting the different sample points directly according to the brightness data, we first calculate some order number from the brightness value of each sample, and find the mean brightness value for each sample. This ordering of samples is simple and is not restricted to the number of channels. Using these two quantities, we should be able to find some discreate clusters from the samples and finally classify the multidimensional image data. Thus, the method is simple, computationally soft, and useful to nonexperts. To show the validity of our method, we applied our proposed algorithm on NOAA satellite image data, as a simple experiment. We were able to classify and separate the plane area and verify the correctness of our method. By plane area we mean areas other than hills and high mountains. Thus, the plane area mainly consists of harvest land and town and city areas. We introduce our idea in the next section, which is followed by an application example.

II. The Basic Method

A. Clustering in the Multidimensional Spatial Distribution

The multidimensional data consists of images received from N different frequency channels. When different image points are plotted in N-dimensional brightness hyperspace, we get an N-dimensional spatial distribution of the image points. A function $P[\alpha_1, \alpha_2, \cdots, \alpha_n]$ is defined that denotes the number of pixels with brightness values α_1 from channel 1, α_2 from channel 2, and so on [6].

The distribution of P in the N-dimensional brightness space is obtained by scanning all brightness images from channel 1 to channel N.

B. Ordering of the Brightness

The image can only be drawn from the visible channel data, by coloring different brightness levels differently. There the basic components such as land and sea are distinguishable, but no significant classification is possible. Even when the component is the same, brightness is not constant over the whole region of the image, for reasons such as that the brightness depends on the angle of the satellite and solar elevation angle, etc. Similarly, the same brightness values do not always mean that they belong to the same category. We need to exploit all the information stored implicitly and in a combined way, in other nonvisible channel images. We proposed an ordering of the composite data to classify it.

In the usual two- and three-dimensional analysis of remote sensing data, clusters are classified by the center of gravity in which each cluster is defined as a collection of closely placed points. So, they suffer from two drawbacks. For visual methods, one can use data from two or at most three channels, as we used in [6]. Also, the range or center of a cluster is not fixed, and depends slightly on the user's choice. In the method proposed here, by proper manipulation, first the multidimensional data is broken into small groups or clusters, distinctly separated. A range of such small clusters was selected and a designated class is attributed to them. The selection of position and range of such clusters, corresponding to a particular class is done in a supervised manner, explained in the next section.

C. O-M Graph

In this section, we describe how we break the multidimensional data into a series of ordered groups. Multidimensional data are considered to be like words consisting of several letters. The letters here are the brightness values from different channels, i.e., channel 1, channel 2, $\cdots$, channel N. Now, the way the words are ordered lexicographycally in the dictionary, we order the multidimensional data in a table. A small part of that table is shown in Table I. We assign a serial order number to every piece of multidimensional data, which is the first column entry of Table I. In the next four columns, the brightness values, as obtained from the four channels, are entered. (Considering the number of channels $N = 4$). The sixth column of Table I is the mean value of brightness received from the four channels. Individually, this average value has no meaning. Quite different data like (1, 1, 100, 100), (100, 100, 1, 1), or (100, 1, 1, 100) will all bear the same meaning. But, combined with the order number, it will be different for all the above examples. (100, 100, 1, 1) will have a much greater order number than (1, 1, 100, 100). In Table I we see for order numbers 223, 229, 235, and 240 we have same average, 21. But, the duple, (order, mean), is different for all four of these entries.

In the last column of Table I, we enter the value of the histogram

Authorized licensed use limited to: TOHOKU UNIVERSITY. Downloaded on March 08,2010 at 01:43:09 EST from IEEE Xplore. Restrictions apply.

TABLE I
PART OF SAMPLE LIST SHOWING THE ORDER OF THE BRIGHTNESS DATA

Order	Channel 1	channel 2	channel 3	channel 4	Mean	P
220	3	4	38	36	20.25	328
221	3	4	38	37	20.50	1014
222	3	4	38	38	20.75	538
223	3	4	38	39	21.00	96
224	3	4	39	33	19.75	26
225	3	4	39	34	20.00	32
226	3	4	39	35	20.25	66
227	3	4	39	36	20.50	393
228	3	4	39	37	20.75	1679
229	3	4	39	38	21.00	1518
230	3	4	39	39	21.25	423
231	3	4	39	40	21.50	25
232	3	4	40	34	20.25	11
233	3	4	40	35	20.50	41
234	3	4	40	36	20.75	264
235	3	4	40	37	21.00	1567
236	3	4	40	38	21.25	2331
237	3	4	40	39	21.50	866
238	3	4	40	40	21.75	108
239	3	4	41	35	20.75	17
240	3	4	41	36	21.00	179
241	3	4	41	37	21.25	1288

Mean: mean value of brightness.
P: histogram function value.

function *P*. For example, the entry 328 in the *P*-column of the first row in Table I simply means that the number of image pixels with a brightness value from channel 1, channel 2, channel 3, and channel 4 as 3, 4, 38, and 36, respectively, is 328. Similar to our previous work [6], where we have used some thinning of sample points to make the boundaries of the clusters clearer, here we use a similar approach. If we list all the multispectral data points in Table I, the range of the order numbers becomes unmanageably great. To deal with this problem, we enter in Table I only those entries for which the *P* value (the histogram function value) is equal to or greater than 10. Thus, only those sample data are entered in Table I, which have occurred at least 10 times or more. We delete entries with *P* values less than 10. Then, we assign serial order numbers (column 1 of Table I) to the entries in Table I. This keeps the order number within a manageable range.

Now, we are ready to plot the multidimensional data on a two-dimensional screen. We plot the two-dimensional data (order, mean) on a graph we will call the O–M graph. We can say that this O–M graph is a two-dimensional persentation of a multidimensional plot. How, using this O–M graph, we could successfully do some supervised classification, is elaborated in the next section.

III. APPLICATION OF O–M GRAPH FOR LAND CLASSIFICATION

A. Description of Data

As an application example, to see the validity of our classification method, we used NOAA AVHRR satellite image data. The data consists of five channels, the wavelength ranges of which are given below [9]:

channel 1: λ = 0.58–0.68 μm (visible)

channel 2: λ = 0.73–1.10 μm (near infrared)

channel 3: λ = 3.55–3.93 μm (infrared)

channel 4: λ = 10.5–11.5 μm (infrared)

channel 5: λ = 11.5–12.5 μm (infrared)

Though the classification method of the O–M graph can handle many channels of data, we restricted our experiment to four channels.

The time of record of the data is 13:00 Hrs Japan standard time (04:00 GMT) on the clear sunny day of November 9, 1988. We used only the first four channels of data received from NOAA-11. The reason behind dropping the channel 5 data during experimentation is that the thermal channels channel 4 and channel 5 have very near λ range, as shown above.

The data collected by the NOAA-11 satellite are obtained by scanning Tohoku, the northern region of Japan. The original image area is 256 × 512 pixels, 1 pixel covering an area of 1.1 (km^2). The choice of area facilitated us the access to some official data from the prefactural office, Miyagi Prefecture in Tohoku being our local region. Thus, some quantitative analyses of the classification results were possible.

The requisite preprocessing of the data, received by NOAA, is done by the Faculty of Science, Tohoku University. The data received from channel 1 to channel 4 were converted to image data by Mercater projection. Channel 1 (visible) and channel 2 (near-infrared) data were converted into albedo, and channel 3 and channel 4 (both infrared) were converted into brightness temperature. The albedo means reflectance. The brightness is multiplied by a suitable factor [10] to get the reflectance from channel 1 and channel 2 data. We received the data after that preprocessing.

B. Normalizing of Image Data

In this study, we normalize the 10-b data to 6 b. Though by reducing from 10 to 6 b we lose some of the information content of the data, we had to do this to perform our experiments within the available memory size. This is done as a preliminary step of experimentation with our algorithm, and a machine with larger memory is expected to give better results.

We adopt a simple algorithm to normalize the brightness data of the channels. This ignores the correlation of visible and thermal bands. Actually, the weight of every channel is to be balanced according to the visual image components. But as a first step, we assume that the weight of all the channels are the same.

For normalization, we first find the mean brightness value for a particular channel from the frequency distribution of the samples. That point is mapped to the middle point of the normalized 6-b data. Then, from the minimum value to the arithmetic mean, and from the arithmetic mean to the maximum value, linear interpolation is used to map 10-b data to 6-b.

C. O–M Graph for Classifying AVHRR Data

We use four channels of data received from NOAA AVHRR. For a particular point (pixel) in the image, we have the data vector consisting of brightness information from channel 1, channel 2, channel 3, and channel 4. Now, the seriality of the entries in Table I is prepared in the order, with channel 1 at the most significant and channel 4 at the least significant position. Finally, those entries of Table I with a *P* value less than 10 are deleted. Now we assign the order number, i.e., column 1 of Table I, serially. Thus, order number changes slowly with a change in the value of the channel 4 data. But small changes in the value of channel 1 data may lead to a large change in order number. In this study, considering that

Authorized licensed use limited to: TOHOKU UNIVERSITY. Downloaded on March 08,2010 at 01:43:09 EST from IEEE Xplore. Restrictions apply.

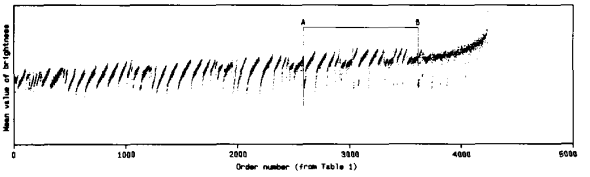

Fig. 1. O–M graph.

channel 1 data is most important, we assigned it the highest priority. In other studies it can be decided differently, depending on the physical meaning of the particular data, using the prior experience of the user. We propose that these two parameters, the order number and the mean value, will map the n-dimensional data points on a two-dimensional computer display, in a way to extract the clusters easily. The O–M graph is shown in Fig. 1. This also allows one to view the whole set of data in the smaller area of the display. The shapes of the groups of points, obtained in this method are small ramps, like the teeth of a saw.

As an application of this four-dimensional analysis method, we tried to extract the plane area of the Tohoku region. We first discuss our classification results qualitatively and then perform some quantitative analysis by comparing with the available data.

While creating the O–M graph, we have assigned channel 1 data the most significant position. This is done rather intuitively, considering that channel 1 being visible may contain the most significant features of the Earth's surface. To assign an image category to the clusters of the O–M graph, we have the following steps.

1) Fix the range of a group of points on the O–M graph by using a pair of vertical cursors on the computer screen. They fix a range of order number. Similarly, by using a horizontal cursor, we can specify a range of the y-axis, i.e., the mean value. And thus, finally we can use a rectangular box to fix the range of selection for the x as well as the y axis of the O–M graph.

2) The portion selected as above can be projected on the image, with the color of choice, as shown in Fig. 2.

3) Compare the result from step 2 on the computer display with a map or topographical data, noting coastline, plane, mountain area, and so on.

This interactive system is made using the graphics tool of an engineering work station and programs in the C language. This method needs only area information from map, and thus facilitates even use by nonexperts with ease.

Following step 2 above, it is found that the groups of points in the range from (A) to (B) as in Fig. 1, correspond to plane areas, by superimposing on the channel 2 image and comparing with the map.

Also, the range from origin to (A) corresponds to sea, coastline and mountain areas. The range beyond (B) are groups of points corresponding only to clouds.

In Fig. 2, the plane area as obtained by selecting the clusters ranging from (A) to (B) of Fig. 1 is shown in green, superimposed on the channel 2 image. Different prefectures of North Japan are demarcated by yellow lines (by using available data). In this case, the channel 2 image is used, because land areas can be recognized most clearly in channel 2 image. The main plane areas in Tohoku region are marked as (A) to (L) in Fig. 2, and are listed in Table II. We see in Fig. 2 that all of the green patches as obtained by our classification algorithm strikingly correspond to the exact locations of the plane areas in the Tohoku region. This qualitatively ensures the correctness of our analysis method.

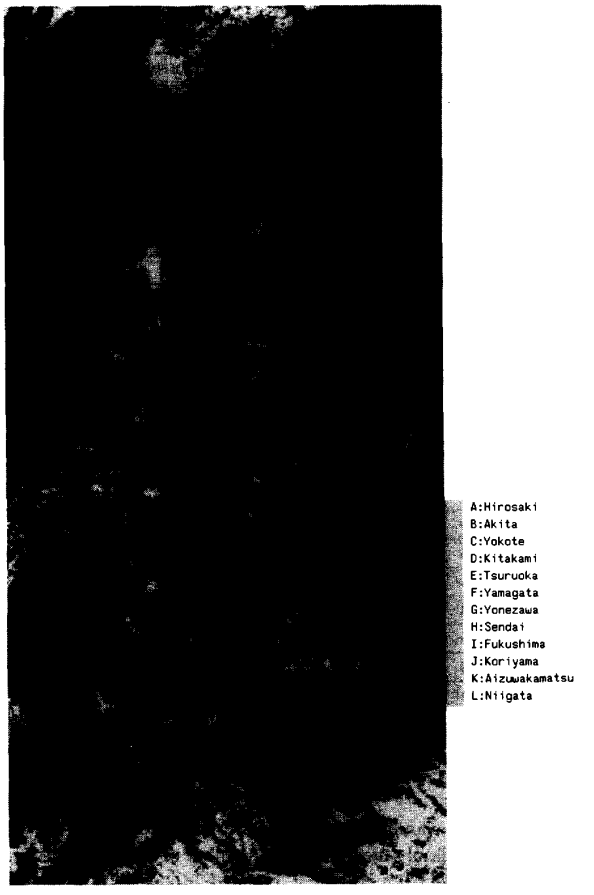

Fig. 2. Plane area as obtained by our analysis colored in green, and superimposed on the channel 2 image.

TABLE II
MAIN PLANE AREAS OF TOHOKU REGION OF JAPAN

Mark	Plane	Main Town
A	Tsugaru	Hirosaki
B	Akita	Akita
C	Yokote	Yokote
D	Kitakami	Kitakami
E	Shonai	Tsuruoka
F	Yamagata	Yamagata
G	Yonezawa	Yonezawa
H	Sendai	Sendai
I	Fukushima	Fukushima
J	Koriyama	Koriyama
K	Aizu	Aizu
L	Niigata	Niigata

D. Quantitative Analysis

The results from the analysis of plane area in Miyagi prefecture were compared with the data [11] available from the Miyagi Prefecture Office, Statistical Division. Table III lists the different clas-

Authorized licensed use limited to: TOHOKU UNIVERSITY. Downloaded on March 08,2010 at 01:43:09 EST from IEEE Xplore. Restrictions apply.

TABLE III
CLASSIFICATION OF LAND IN MIYAGI PREFECTURE [11]

Class	Area (km^2)
Agriculture	1515.71
(in rice field)	(1204.90)
(in farm)	(307.54)
Forest	4235.48
(in private)	(2897.52)
Waste field	20.81
Water channels	318.60
(in river)	(204.16)
Road	270.52
(in thoroughfare)	(174.04)
Building land	370.78
(in living)	(231.39)
(in industrial)	(21.97)
Others	559.79
Total	7291.69

TABLE IV
COMPARISON OF RESULTS OBTAINED USING O-M GRAPH ANALYSIS

	This Study (km^2)	Statistical [11] (km^2)
Miyagi Pref.	7,279	7,292
Plane Area †	2,132	2,157

†Plane area: total of agriculture, road, and building land.

sifications of land area obtained from these data. In Table III, the figures are not always the absolute correct values, and includes observational errors and some presumed values. The summation of different classes (including "Others") are adjusted so as to be the same as the total area of Miyagi prefecture. Thus, the estimation as obtained from Table III is only a first approximation and not the exact values.

As agricultural areas, residential quarters, and roads generally correspond to the plane area, we add these items to approximately obtain the total plane area. The map of the Tohoku region with prefecture boundaries was overlaid on the image by matching the distinguishable promontories and small islands. Table IV compares the results. The area of Miyagi prefecture calculated from pixel counting was found to be quite close to the official data. This means that the boundary and the geometric rectification of the image by Mercator projection is accurate. Therefore, it is acceptable to be used for area calculations. The plane area in Miyagi prefecture, colored in green in Fig. 2, was almost the same as the area obtained from the prefecture office. The error was about 1.16 percent. This value of the error is negligibly small, considering the inherent sources of errors in the statistical data obtained from the Miyagi Prefecture Office, and in our consideration of plane area.

IV. DISCUSSION

For multidimensional analysis of image data, in remote sensing the maximum likelihood method is commonly used. But the maximum likelihood method is useful in cases when the different image categories are clearly separated due to the high resolution of the received data, as in the case of land classification using LANDSAT data [12]. However, expert knowledge is required to categorize the NOAA data, because of the larger area covered by single pixels and there is some confusion in categorizing the different image points.

On the other hand, the method proposed in the present study is easy to use, even for a nonexpert, when classifying the image categories, using the patterned groups of points in O-M graph. This system also provides a convenient man-machine interface (windows, mouse, cursor, and so on) for the classification, and displays the classified results in a colored visual image and that enables us to compare the result with the related information directly [13]. In spite of the lower spatial resolution of the NOAA AVHRR data, we could obtain a relatively accurate result through our analysis.

Before the three-dimensional classification started, the objects were identified using the spectral wavelength band. Therefore, the operator's knowledge of spectral properties was used. On the contrary, we have developed the O-M graph method, in which essentially no one need look at the multidimensional spatial distribution of data. The O-M graph is a visual pattern on the two-dimensional screen of the clusters present in the multidimensional spatial distribution of data.

Here, we cut or neglected those points, i.e., pixels in the image, for which the occurrence was less than 10, i.e., the histogram function value $P < 10$. We have calculated that by doing this we neglected only 0.007 percent of the total 256×512 pixel image points. On the other hand, we could save a lot in the range value of order number, and thus would be able to squeeze the O-M graph onto the display screen.

NOAA data are usually overlapped in the multidimensional brightness space, as is discussed in [6]. In [6] the boundaries became clear by thinning the sample points. We use a similar technique here, by neglecting those samples for which the occurrence frequency $P < 10$, and could get groups of samples that are clearly separated in the O-M graph.

Because of the low resolution per pixel, or in other words, the large area covered by a single pixel, by using NOAA AVHRR data we cannot have a close classification of land area. For a broader classification of land area, the method we introduced in the communication is a very useful tool for nonexperts, and at the same time is user-friendly and fast.

V. CONCLUSIONS

In this study, we proposed a new multidimensional analysis method, and as an experiment applied the method to the classification of the multispectral NOAA AVHRR image data. We did some classification of land areas using this method. The obtained results were compared to the actual survey data and found to be quite close, proving the correctness of the approach.

ACKNOWLEDGMENTS

The image data were processed by "cips" installed at Computer Center, Tohoku University.

REFERENCES

[1] M. Niimi, S. Kamata, and E. Kawaguchi, "A clustering method using a Hilbert scanning in multidimensional feature space," IEICE, Tech. Rep. PRU 92-103, pp. 9-15, 1993.

[2] C. E. Livingstone, K. P. Singh, and A. L. Gray, "Seasonal and regional variations of active/passive microwave signatures of sea ice," *IEEE Trans. Geosci. Remote Sens.*, vol. 25, pp. 159-173, Mar. 1987.

Authorized licensed use limited to: TOHOKU UNIVERSITY. Downloaded on March 08,2010 at 01:43:09 EST from IEEE Xplore. Restrictions apply.

[3] A. A. Green and M. Berman, "A transformation for ordering multispectral data in terms of image quality with implications for noise removal," *IEEE Trans. Geosci. Remote Sens.*, vol. 26, pp. 65–74, Jan. 1988.
[4] J. Bryant, "On displaying multispectral imagery," *Photogram. Eng. Remote Sens.*, vol. 54, no. 12, pp. 1739–1743, 1988.
[5] J. M. Durand and Y. H. Kerr, "An improved decorrelation method for the efficient display of multispectral data," *IEEE Trans. Geosci. Remote Sens.*, vol. 27, pp. 611–619, Sept. 1989.
[6] J. Kudoh and S. Noguchi, "A study of three-dimensional histogram of the NOAA AVHRR images," *IEEE Trans. Geosci. Remote Sens.*, vol. 29, pp. 736–741, Sept. 1991.
[7] ——, "Identification of fog with NOAA AVHRR images," *IEEE Trans. Geosci. Remote Sens.*, vol. 29, pp. 704–709, Sept. 1991.
[8] J. C. Barnes and M. D. Smallwood, *TIROS-N/NOAA Series Direct Readout Services Users Guide*, Washington, D.C.: NOAA, Commerce, 1982.
[9] L. Lauritson, G. J. Nelson, and F. W. Porto, "Data extraction and calibration of TIROS-N/NOAA radiometers," NOAA, Tech. Memo. NESS1077, 1979.
[10] H. Kawamura, "Tohoku image database: TIDAS," *SENAC*, vol. 26, no. 3, pp. 48–56, 1993.
[11] "The Heisei, 2nd edition," in *The Statistical Year Book of Miyagi Prefecture*. Miyagi, Japan: Miyagi Prefecture Statistical Div. 1991.
[12] K. S. Fu, "Pattern recognition in remote sensing of the Earth's resources," *IEEE Trans. Geosci. Remote Sens.*, vol. 14, pp. 10–18, Jan. 1976.
[13] S. Obata, S. Matsuzawa, H. Kawamura, and S. Noguchi, "Mapping geographical information to NOAA image data," in *Proc. 40th Annu. Conv. ISP Japan*, 1990, p. 567.

The Los Alamos Beacon Receiver Array

R. C. Carlos and R. S. Massey

Abstract—**We describe radio receivers that monitor transmissions from beacons on geosynchronous satellites. The receivers can detect perturbations of a 300–3000 s period in the electron density integrated from beacon to receiver, for amplitudes as low as (1–2) $\times$ 10^{13} m^{-2}. Data are used in studies of atmospheric acoustic and acoustic-gravity waves.**

Introduction

In this communication we describe the operation of phase-measuring receivers developed to measure small fluctuations in the line integral of the ionospheric electron density (called total electron content, abbreviated TEC). The fluctuations of interest, in the frequency range 0.3–30 mHz and having wavelengths from a few kilometers to a few hundred kilometers are caused by acoustic and gravity waves in the neutral atmosphere that perturb the local plasma. We are interested in studying both the natural background of acoustic and acoustic-gravity waves, for which the sources are not generally known, as well as waves produced by known sources such as large explosions and launches of large rockets. The natural background studies require a fixed, two-dimensional array with baselines as long as 90 km, operating continuously. Studies of man-made sources, by contrast, require easily deployable arrays of autonomous stations in a variety of geometries, some with separations of hundreds of kilometers.

The usefulness of radio beacons on satellites for measuring ionospheric parameters was recognized soon after the first satellites were launched [1]. A variety of techniques have been developed and used for measuring fluctuations of the TEC, each with advantages and disadvantages for our purposes. A large body of literature, typified by [2]–[7], described observations made by measuring the Faraday rotation of the received signal from a radio beacon on a low-earth-orbit or geosynchronous satellite. Faraday-rotation instruments are sensitive to TEC fluctuations as low as about 10^{15} m^{-2} [7], are portable, and can operate with present radio beacons transmitting on a single frequency from geosynchronous satellites (e.g., ATS-3, GOES-2, and MARECS-B). Another technique is to measure the differential phase between phase-locked VHF beacons at different frequencies (see [8]–[10]). Fluctuations in TEC have also been observed by measuring amplitude scintillations in received signals from beacons on geostationary satellites [11], but these do not provide quantitative information on the amplitude of the fluctuation. Phase fluctuations in signals from celestial sources [9]–[10] have been used to measure TEC fluctuations as small as 10^{14} m^{-2}, but this technique requires large antennas to obtain adequate signal-to-noise ratios. Elkins [12] surmounted this problem by measuring phase fluctuations in signals from single-frequency radio beacons on geostationary satellites, and was able to observe TEC fluctuations as small as 2×10^{13} m^{-2} using two receivers separated by 10 km. Elkins used a microwave link between the two receivers to provide the required phase reference.

Our requirements have been met by extending the technique of Elkins, using newly available rubidium oscillators at each receiver to avoid the need for microwave links. The phase stability of these oscillators is adequate to resolve TEC fluctuations as small as (1–2) $\times$ 10^{13} m^{-2} between sites of arbitrary separation. We have also implemented a novel scheme for digitally demodulating the phase at each site, and transmitting only the demodulated phase samples at sampling rates of 0.1 Hz from the remote sites to a base station, rather than having to transport samples of the signal itself. We thereby reduce the size of a day's data file from 34 megabytes to about 40 kilobytes without loss of information in the bands of interest. In the next section we provide details of our method.

Method

Carrier phase measurements depend on the existence of satellite radio beacons with frequencies well above the highest plasma frequency along the path. Beacons on geosynchronous or slowly moving satellites are needed to avoid confusion between real propagating waves and apparent waves caused by ray-path motion across stationary ionospheric structures. In order for the path to be approximately the geometric path, frequencies above 100 MHz are required. At these frequencies, the received phase is approximately

$$\Phi_r = \Phi_s + \frac{2\pi f r}{c} - \frac{kN_e}{f}\beta + \Phi_0 \quad (1)$$

where Φ_r is the phase measured at the receiver, Φ_s is the phase at the satellite, f is the received frequency (hertz), r is the range from the satellite to the receiver, k is a constant, Φ_0 is the phase offset through the receiver system, and N_e is the TEC. TEC is defined by

$$N_e = \int n_e \, ds \quad (2)$$

Manuscript received March 22, 1994; revised April 4, 1994. This work was supported by the U. S. Department of Energy.

The authors are with the Los Alamos National Laboratory, Los Alamos, NM 87545.

IEEE Log Number 9402673.

0196-2892/94$04.00 © 1994 IEEE

Authorized licensed use limited to: TOHOKU UNIVERSITY. Downloaded on March 08,2010 at 01:43:09 EST from IEEE Xplore. Restrictions apply.